Arabian Journal of Geosciences (2019) 12: 407
https://doi.org/10.1007/s12517-019-4568-9

ICCESEN 2017

A comprehensive characterization of North China tight sandstone using micro-CT, SEM imaging, and mercury intrusion

Zhilin Cheng[1] · Zhengfu Ning[1] · Huawei Zhao[2] · Qing Wang[1] · Yan Zeng[1] · Xiaojun Wu[1] · Rongrong Qi[1] · Shuang Zhang[1]

Received: 29 October 2018 / Accepted: 12 June 2019 / Published online: 25 June 2019

Abstract

A clear understanding of pore structure of tight oil reservoirs is essential for reservoir evaluation and enhanced oil recovery. This paper presents a multiscale characterization method using a combination of pressure-controlled porosimetry (PCP), micro-computed tomography (micro-CT), and scanning electron microscopy (SEM). Four tight sandstone samples from Chang 7 Formation in the Ordos Basin were collected for petrophysical characterization. Pore-throat size distributions (PTSDs) for these samples were measured via PCP. A high-resolution micro-CT scan (1 μm/pixel) was used to acquire 3D volumetric images of small core plugs to evaluate pore connectivity of these samples. Additionally, high-resolution digital images were obtained through SEM to identify different pore types. SEM analysis shows that pores in tight sandstones could be classified into four types, i.e., residual interparticle pores, grain dissolution pores, clay pores, and micro-fractures. Residual interparticle pores are often coated by fibrous illite and chlorite. Grain dissolution pores are mainly deduced from the dissolution of grain minerals, among them the feldspar dissolution pore is the primary type. According to the PCP experiments, these samples exhibit multiscale pore structures with a wide range of PTSD from 9.2 nm to 500 μm dominated by nanopores. Average mercury intrusion saturation and permeability contribution value of the dominating nanopores are 63.61% and 80%, respectively. Given the unresolved nanopores, CT images were segmented into three phases, including pore space, grain phase, and clay minerals. The results of connectivity analysis demonstrate that macroscopic pores are mostly connected by clay phases, implying that nanopores provide the critical flow paths. This novel multiscale characterization approach provides us a better understanding of complex pore structures of tight sandstones.

Keywords Tight sandstone · Pore structure · Multiscale characterization

PACS 61.05.−a · 61.05. cp · 87.16. dp · 81.70. Tx

Introduction

With increasing demand for energy and continuing depletion of conventional oil and gas resources, hydrocarbons in unconventional reservoirs have attracted significant attention and become a crucial alternative energy source (Cheng et al. 2018; Song et al. 2018; Huang et al. 2018). Recent advances in the less-expensive fracking technology and large-scale industrial applications have led to the increase of the production rate of hydrocarbons from unconventional resources and the extent of technically recoverable reserves (Hughes 2013). Tight oil is light oil stored in unconventional formations with extremely low porosity and permeability, which makes it difficult to be recovered. Generally, the petrophysical properties of rocks are greatly dependent on its pore structure characteristics (Cheng et al. 2019; Yang et al. 2014, 2016). Therefore, a systematic characterization of pore structure of tight oil reservoirs is fundamental to understand the fluid seepage mechanism inside pore space and may provide insights into the successful development of such tight reservoirs.

This article is part of the Topical Collection on *Geo-Resources-Earth-Environmental Sciences*

✉ Zhilin Cheng
zhilin_cheng1992@163.com

✉ Zhengfu Ning
nzf@cup.edu.cn

[1] China University of Petroleum-Beijing, School of Petroleum Engineering, Beijing, China

[2] SINOPEC Petroleum Exploration and Production Research Institute, Beijing, China

The popular techniques used to quantitatively or qualitatively determine the pore structure of tight rocks mainly contain SEM, focused ion beam (FIB)-SEM, micro-CT, PCP, rate-controlled porosimetry (RCP), N_2 gas adsorption (N_2GA), nuclear magnetic resonance (NMR), and small-angle neutron scattering (Lai et al. 2018; Zhao et al. 2015). In the past few years, with the help of these advanced techniques, many research groups have concentrated on the evaluation of pore structure of unconventional rocks, such as shales (Yang et al. 2014, 2016), coals (Heriawan and Koike 2015; Li et al. 2017), and tight oil/gas sandstones (Gao and Li 2016; Zhao et al. 2015; Lai et al. 2018). For the significant advances in this topic, one can refer to several systematic publications (Ougier-Simonin et al. 2016; Mathews et al. 2017; Lai et al. 2018). In this study, we only focused on the features of pore structure of tight sandstones. An important aspect for tight sandstones is the considerable clay contents found on rock matrix. The ubiquitous clay minerals in tight rocks are usually associated with abundant micro-pores, which reduces the porosity and permeability and results in complex pore structures for tight reservoirs. To be specific, tight sandstones generally exhibit a multiscale pore structure, which is quite different from that of medium-high and high-permeability sandstones with unimodal pore size distributions. For conventional reservoirs, because of the relatively narrow pore size distribution (ranging from several to tens of microns), its pore structure can be determined by using only one technique such as micro-CT. In contrast, pore sizes of tight sandstone vary widely from several nanometers to dozens of microns with the nanopores being the dominating type (Liu et al. 2017; Zou 2017; Zhao et al. 2018). Apparently, the nanopores in tight samples cannot be resolved by micro-CT. Furthermore, other characterization methods also have cons and pros (Nelson 2009). SEM has been widely applied in geological research to investigate micro-porous limestones and fine-grained clay stones (Marszałek et al. 2014; Vázquez et al. 2013; Zhao et al. 2018); it can give direct observations about pore morphology and mineral types, but fails to provide quantitative data. CT imaging provides a non-destructive approach to extract 3D structural information of geomaterials at micron to millimeter scale, even the nanoscale (Bultreys et al. 2016; Bai et al. 2013). However, to our knowledge, currently it cannot detect nanopores smaller than 50 nm (Bai et al. 2013). Besides, to acquire high-resolution CT images, the sample size must be small enough to ensure the narrow field of view (Blunt et al. 2013). Hence, in this case, the small sample may be not representative for heterogeneous tight sandstones. Likewise, FIB-SEM can quantitively reveal the pore-throat features at the nanoscale; but unlike CT tests, FIB-SEM experiments cannot be repeated and are always restricted by the high expenses. In addition, N_2GA and small-angle neutron scattering can only capture the information of the majority of nanopores. For PCP method, although more mercury can be forced into rock samples through the high-pressure injection, it cannot tell the pores and throats in rock samples. As such, even though RCP can distinguish the information of pores and throats, it cannot detect more tiny pores because of the low injection pressure. NMR is a fast and non-destructive technique for the determination of pore structure and fluid flow characteristics for tight rocks. However, conversion coefficient of the T2 spectrum is not general and needs to be rigorously calculated.

Because tight sandstone is of high complexity and heterogeneity, the accurate assessment of structural characteristics of tight rocks is impossible only through a single technique. Developing a reasonable and reliable technique to understand the overall structural characteristics appears to be necessary and urgent. Thus, recently, researchers have attempted to seek a combination of several complimentary approaches to address these research gaps. Zhao et al. (2015) applied PCP and RCP methods to investigate the pore systems of tight sandstones in the Yanchang formation, and they also corrected a permeability estimation model based on mercury intrusion data. Cao et al. (2016) performed mercury intrusion and N_2GA experiments to explore the geological control factors of complex pore structure for tight sandstones. They demonstrated that intercrystalline pores developed in clay have minor contributions to porosity, and confirmed the good applicability of the N_2GA hysteresis loop in describing pore shape in tight rocks as well. Additionally, one study by Dianshi et al. (2016) combined RCP and NMR experiments to probe the size distributions of pores and pore throats in tight sandstones. In their study, the limitations of RCP in representing the pore size and pore-throat ratio were elucidated, and those were addressed by subtracting the throat size distribution from NMR. In a follow-up study, Liu et al. (2017) proposed a multi-scale workflow to characterize pore geometry, size, and connectivity. This workflow involved the high-resolution SEM technique, low-resolution micro-CT, and NMR method. They showed that the permeability and electrical properties of tight rocks are more dependent on the pore structure than porosity. Very recently, through the use of SEM, PCP, and RCP, Gao et al. (2019) obtained the overall pores and pore-throat size distributions and proposed five types of pore throats. Further, they highlighted the significant role of pore-throats in controlling the permeabilities of tight media.

The purpose of this investigation is to illustrate the signatures of pore structure of tight oil sandstones, involving the characterization of pore types, pore size, pore-throats, and pore connectivity. In addition, the effects of pore structure on flow potential and storage capacity of tight rocks were also discussed. The paper has been organized in the following way. Experimental materials and methods were introduced in Section 2. The results of various methods (SEM, micro-CT, and PCP) and implications on petrophysical properties of tight samples were presented in Section 3. Finally, some conclusions were drawn in Section 4.

Table 1 Porosity, permeability, and XRD results of selected samples

Sample	Depth/ m	Poro/ %	Perm/ mD	XRD									
				Qz/ %	Fsp/ %	Cal/ %	Dol/ %	Py/ %	Gp/ %	Clay/ %	I/S/ %	Ilt/ %	Chl/%
YC5	1906.8	13.10	0.444	33.4	42.1	0.7	4.4	/	/	19.4	23	9	68
YC6	1821.9	12.90	0.386	30.2	41.0	7.9	3.9	0.3	0.4	16.3	26	5	69
T2	1594.5	6.98	0.053	36.4	35.2	4	/	/	/	24.4	20	9	71
Z211	1550.0	9.51	0.117	52.9	16.1	2.1	10.6	/	/	18.3	47	23	30

The above abbreviations for the rock minerals referred to the work of Whitney and Evans (2010). Part of the data are from references (Zhao et al. 2015, 2016).

Experimental methods

Samples and experiments

Four water-wet tight sandstone samples were studied in this paper. These cores were taken from different depths of the Upper Triassic Yanchang tight oil reservoirs of the Ordos Basin in northern China, which are core areas of tight oil reservoirs (Zou 2017). The samples were polished into cylindrical core plugs with a diameter of ~ 25 mm and length of 50 mm and then were cleaned using solvent to remove the residual oil. Afterwards, all rock samples were put into a thermotank at 105 °C for 24 h before experiments. All experimental techniques include helium porosity, nitrogen permeability tests, XRD, PCP, SEM, and micro-CT experiments. The properties of the rock samples are shown in Table 1. Note that in our previous studies (Zhao et al. 2015, 2016), the combined PCP and RCP characterization method had been proposed to investigate the full PTSDs and estimate the permeabilities of these tight rocks. For the detailed experimental methods, one can refer to Zhao et al. (Zhao et al. 2015, 2016). Thus, in this work, we only describe the procedures of micro-CT imaging experiments (Section 2.2).

Micro-CT and image processing

Tomographic datasets were obtained using the micro-CT scanner built at State Key Laboratory of Petroleum Resource and Prospect-iRock Technologies (Xiamen) Limited Joint Laboratory of Nano Rock Physics. The scans were conducted on a 2.0-mm plug of each rock using a high-resolution MicroXCT-200 scanner equipped with 80 kV and 8 W X-ray source. The experimental time for a single-core plug lasted for approximately 20 h. Then, a set of 1968 × 2014 × 2000 volumetric images (at 1-μm voxel resolution) for each sample was acquired.

Before image analysis, the original volumetric images need to be filtered with non-local means filter (built in Avizo, FEI) to reduce unnecessary noise (Munawar et al. 2018). This filter is more robust than others when dealing with noisy data, and can effectively preserve the edge features in the image

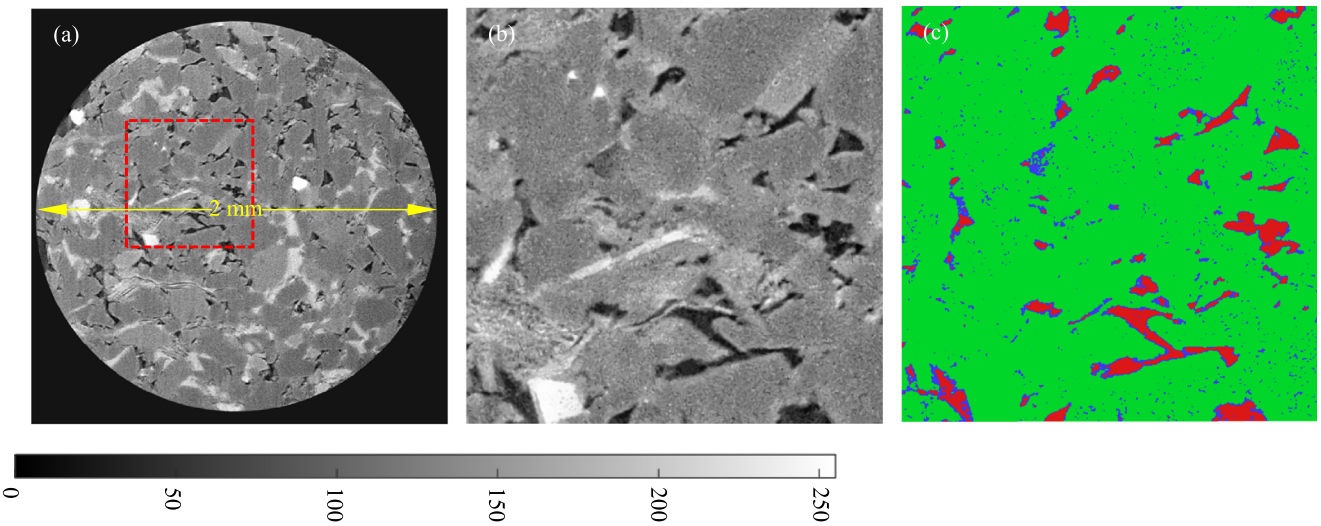

Fig. 1 An example of sample Z211. (a) The original grayscale image; (b) the cropped digital image which has been denoised; (c) the multi-threshold segmented images

Table 2 The range of threshold of each phase for these samples

CT sample	Size / voxel	Grayscale values			Macroporo /%	Total poro /%	Measured poro /%
		GP	CP	Ske			
YC5	600^3	0–65	66–103	104–255	4.07	12.34	13.1
YC6	600^3	0–85	86–108	109–255	5.57	11.81	12.9
T2	600^3	0–75	76–95	96–255	4.63	8.28	6.98
Z211	600^3	0–70	71–100	101–255	2.95	9.96	9.51

where GP and CP represent granular and clay pores, respectively. Ske means the skeleton phase.

(Buades et al. 2005). A typical example was shown in Fig. 1 a and b. The dark color represents the pore phase, while the light one denotes the mineral phase. Following this, because the abundant nanopores cannot be resolved by micro-CT, thus,

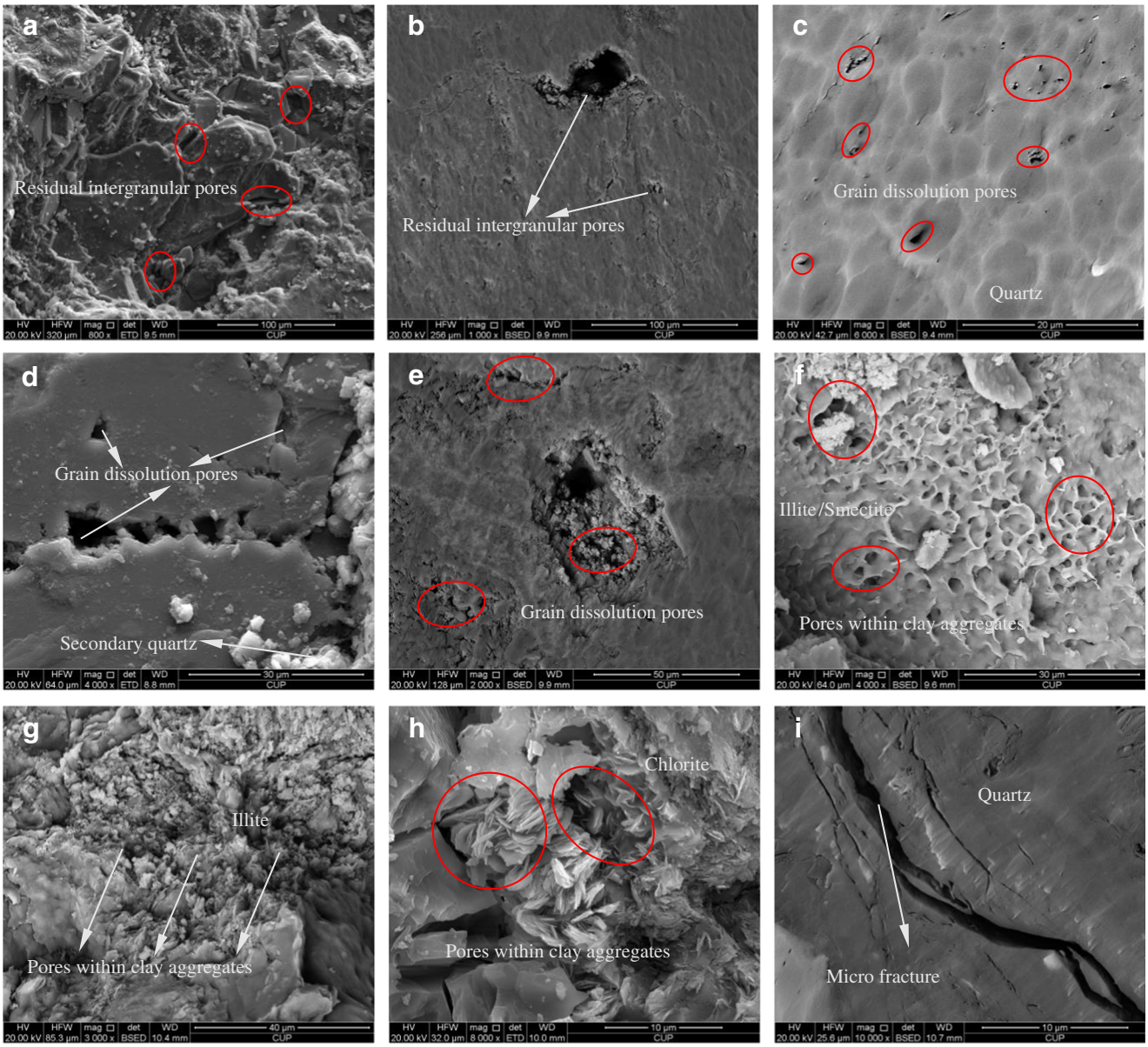

Fig. 2 Representation of the typical pore types in tight sandstone samples. (a) and (b) denote the residual intergranular pores; (c)–(e) show the dissolution pores within the brittle minerals; (f)–(h) represent the clay nanopores; (i) displays the micro-fractures

the classical binary image segmentation cannot be applied. Conversely, the 8-bit datasets were artificially segmented into three phases, as depicted in Fig. 1c, where the green part denotes skeleton, the red is for residual interparticle pores (also namely macropores), and the blue represents the clay phase. The detailed threshold ranges for each phase were listed in Table 2. Then, the macroporosity (granular pores) and micro-porosity (clay minerals phase) can be calculated, also shown in Table 2. After segmentation, Avizo software was used for the visualization of these reconstruction 3D images.

Results and discussion

SEM and XRD analysis

The selected samples are mainly gray to dark-gray fine-grained sandstones. From Table 1, we can see that these samples are rich in quartz (30.2–52.9%), feldspar (16.1–42.1%), and clays (16.3–24.4%). Their compositions account for larger than 90%. Additionally, the primary clay minerals are I/S, illite, and chlorite; among them, the dominant one is chlorite (average proportion can reach approximately 70%, except for Z211). The relative high clay content is a distinctive feature for tight sandstones.

Additionally, according to the results of SEM analysis presented in Fig. 2, pores with various shapes in tight sandstone could be classified into four types, i.e., residual interparticle pores, grain dissolution pores, clay pores, and micro-fractures. To be specific, residual interparticle pores mainly include primary pores after diagenesis process and cemented pores coated with clays such as fibrous illite and chlorite (Schieber 2010). This kind of pores is relatively scattered and rare but large in size ranging between 64 and 400 μm (Loucks et al. 2009). Grain dissolution pores are generated from the dissolution of grains, like quartz, calcite, and feldspar, and feldspar contributes the majority of contribution. Besides, the dominating type within these tight samples is clay pores, which are abundant and develop in various clay minerals (Fig. 2f–h). The pore size distribution ranges from 112 to 600 nm (Zhao et al. 2015), also namely submicron pores (0.1–1 μm). In addition, we also found the existence of brittle micro-fractures, which are usually generated along with brittle minerals (Dürig et al. 2012). The widths of micro-fractures are generally in the nanometer range.

Mercury intrusion characterization

To obtain the PTSDs of tight sandstones, PCP experiments were performed, and the results are shown in Fig.3. It is seen that the maximum intrusion pressure can reach more than 80 MPa, indicating the existence of nanopores. A higher

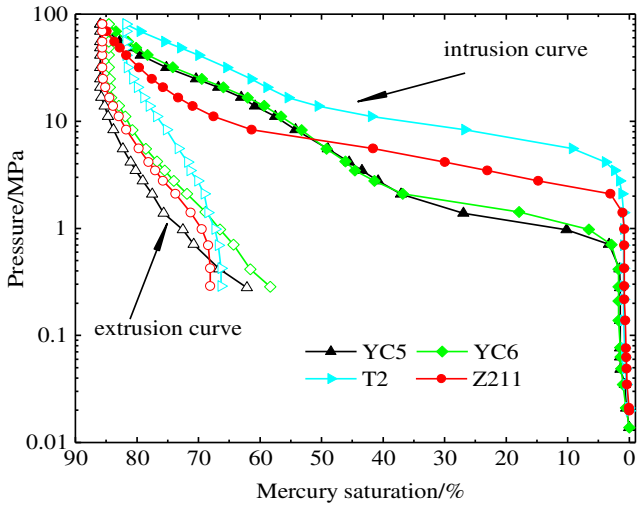

Fig. 3 Intrusion and extrusion curves of PCP for four samples

intrusion pressure corresponds to the lower permeability sample. For example, T2 has the lowest permeability but the highest intrusion pressure. The average intrusion mercury saturation was approximately 80%, showing that there is still unoccupied pore space. This can also be confirmed by the varying trend of the intrusion curve at the end, where the slope of the curve is not parallel to the vertical axis. Furthermore, the rapid increase in the pressure at the early stage is commonly caused by the shielding effects of small pores (Kaufmann et al. 2009), which may reduce the amounts of large pores. Although the intrusion saturation is relatively high, the maximum extrusion saturation is low, implying a large amount of mercury was trapped in rock samples, which could be attributed to a large pore-throat discrepancy.

Through the use of the Washburn equation (Washburn 1921), the PCP intrusion curves can be converted into the PSD curve (see Fig. 4). Additionally, the PCP-derived properties such as the cumulative mercury intrusion saturation curve (storage capacity) and cumulative permeability contribution curve (flow potential) as a function of pore-throat size were also presented in Fig. 4. It is found that the tight sandstone exhibits a multiscale pore structure with pore size ranging from 9.2 nm to 500 μm. The dominated pore-throats mainly distribute from 0.04 to 0.3 μm, see the black line shown in Fig. 4.

When mercury is forcibly injected into the core sample, the curves of cumulative permeability contribution first experience a stable stage, which is almost negligible; then, they increase rapidly and show a very steep trend, as seen in Fig.4. In contrast, the cumulative intrusion mercury saturation curves vary in a different way. After the early stage of the mercury injection, they show a relatively slow increase. Furthermore, it is found that the primary contribution for flow potential is only attributed to a small part of the pore-throats (almost account for the entire flow contribution), but these pore-throats only contribute 15–40% to the cumulative

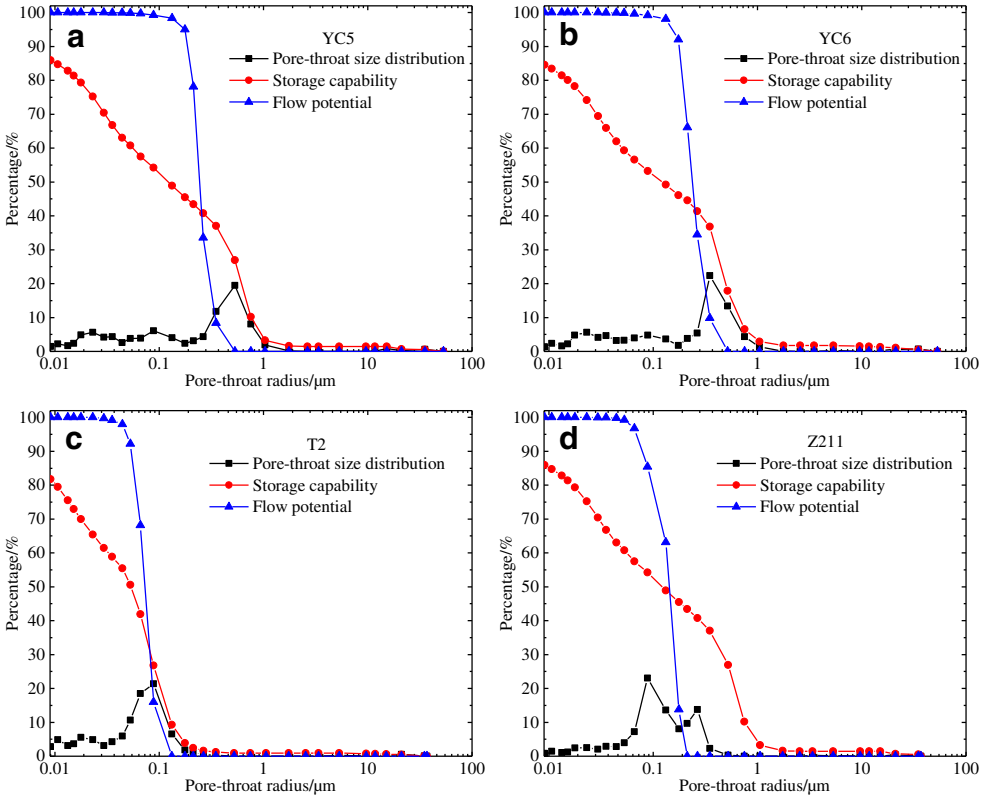

Fig. 4 The pore-throat distributions and the specific contributions of different sized pore-throats on porosity and permeability for these samples

storage. Furthermore, although smaller pore-throats (< 0.1 μm) have negligible contribution to the reservoir flow potential, they are crucial for the reservoir storage capability. This conclusion is consistent with the findings reported by Xi et al. (2016).

Pore connectivity analysis

As mentioned in the "Micro-CT and image processing" section, the volumetric images were segmented into three phases. Subsequently, the macroporosity and the total porosity for each sample can be determined, listed in Table 2. The total porosities calculated from the 3D images were in good agreement with the measured porosities. The resolved porosities, i.e., macroporosities are far less than the total porosities, which is expected due to the unresolved nanopores at this resolution.

To acquire an intuitive recognition of the complex pore space within the tight rocks, taking YC5 as an example, the segmented 3D images are plotted in Fig. 5. It is apparent that the distribution of resolved macropores is isolated, and the pore space consists of isolated pore clusters that cannot merge into an integrated percolated channel. Actually, those pore clusters are almost connected by unresolved small-size throats, and this can be evidenced by the results presented in Fig. 5c. When the clay phase is plotted together, percolated

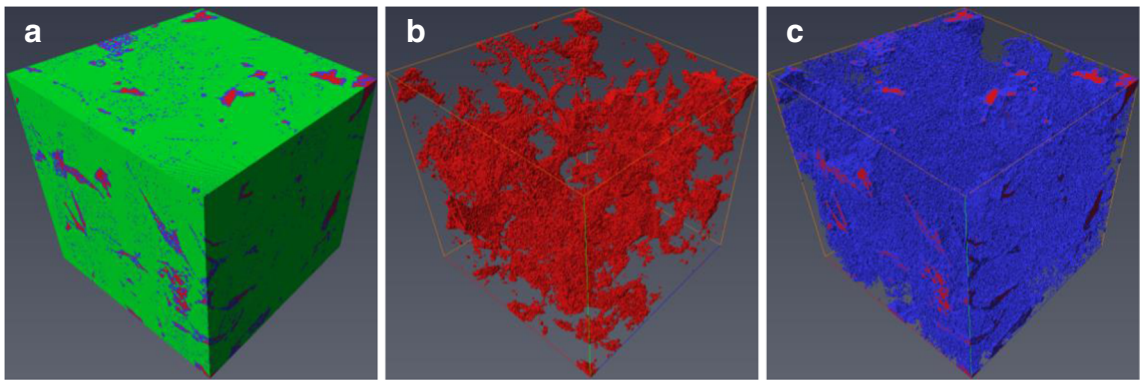

Fig. 5 Volume of (a) the representative element of YC5, (b) resolved intergranular pores, and (c) the combination of the unresolved clay phase and the resolved pores

pathways are found, which implies that the nanopores in clay clusters will determine the transport properties in tight sandstones. Moreover, due to the low contribution of macropores to the pore pace and the dominant role of clay nanopores in determining the flow capacity, tight sandstone always has a very low permeability (Liu et al. 2017).

Conclusion

In this study, a combination of SEM, micro-CT, and PCP was applied to characterize pore structure and understand its effects on petrophysical properties of tight sandstones. The main conclusions are drawn as follows:

1. Tight sandstone samples are rich in quartz, feldspar, and clays, and the summation of them contributes larger than 90% to the rock minerals. Additionally, the pore structure of tight sandstone is highly intricate, which mainly involves four pore types, i.e., residual interparticle pores, grain dissolution pores, clay pores, and micro-fractures. The dominant pore type is clay nanopores, and the considerable content of clays is very favorable to the preservation of such nanopores.
2. Tight sandstone exhibits a multiscale pore structure with pore-throats ranging from several nanometers to hundreds of microns. The size of interparticle pores generally lies in the micron range, but is rare and distributed in rock matrix in an isolated state. Furthermore, the nanopores (< 0.1 μm) have little effect on the flow capacity but play a significant role in controlling the fluids storage. As such, the flow potential for tight sandstones is determined the submicron pore-throats.
3. Given the limited resolution of micro-CT instrument, nanopores in 3D images cannot be effectively detected. Thus, the entire digital rock was classified into three phases, i.e., clay minerals, rock skeleton, and pore phase. Based on the connectivity analysis with the 3D visualization, percolated pathways in pore space cannot be formed only by the resolved intergranular pores. However, nanopores in clay phase bridge the isolated intergranular pores, controlling the main flow paths for tight sandstones.

Funding information The authors would like to thank the National Natural Science Foundation of China (Grant No. 51504265, 51474222 and 51774298) and PetroChina Innovation Foundation (2017D-5007-0205) for the financial support.

References

Bai B, Zhu R, Wu S, Yang W, Gelb J, Gu A, Zhang X, Su L (2013) Multi-scale method of nano(micro)-CT study on microscopic pore structure of tight sandstone of Yanchang Formation, Ordos Basin. Pet Explor Dev 40(3):354–358 http://www.sciencedirect.com/science/article/pii/S1876380413600427

Blunt MJ, Bijeljic B, Dong H, Gharbi O, Iglauer S, Mostaghimi P, Paluszny A, Pentland C (2013) Pore-scale imaging and modelling. Adv Water Resour 51:197–216

Buades A, Coll B, Morel J-M (2005) A non-local algorithm for image denoising. Proc., 2005 IEEE computer society conference on computer vision and pattern recognition (CVPR'05)60–65

Bultreys T, De Boever W, Cnudde V (2016) Imaging and image-based fluid transport modeling at the pore scale in geological materials: a practical introduction to the current state-of-the-art. Earth Sci Rev 155:93–128

Cao Z, Liu G, Zhan H, Li C, You Y, Yang C, Jiang H (2016) Pore structure characterization of Chang-7 tight sandstone using MICP combined with N 2 GA techniques and its geological control factors. Sci Rep 6:36919

Cheng Z, Wang Q, Ning Z, Li M, Lyu C, Huang L, Wu X (2018) Experimental investigation of countercurrent spontaneous imbibition in tight sandstone using nuclear magnetic resonance. Energy Fuel 32(6):6507–6517. https://doi.org/10.1021/acs.energyfuels.8b00394

Cheng Z, Ning Z, Wang Q, Zeng Y, Qi R, Huang L, Zhang W (2019) The effect of pore structure on non-Darcy flow in porous media using the lattice Boltzmann method. J Pet Sci Eng 172:391–400 http://www.sciencedirect.com/science/article/pii/S0920410518308210

Dianshi X, Shuangfang L, Zhengyuan L, Huang W, Meiwei G (2016) Combining nuclear magnetic resonance and rate-controlled porosimetry to probe the pore-throat structure of tight sandstones. Pet Explor Dev 43(6):1049–1059

Dürig T, Mele D, Dellino P, Zimanowski B (2012) Comparative analyses of glass fragments from brittle fracture experiments and volcanic ash particles. Bull Volcanol 74(3):691–704

Gao H, Li HA (2016) Pore structure characterization, permeability evaluation and enhanced gas recovery techniques of tight gas sandstones. J Nat Gas Sci Eng 28:536–547

Gao H, Cao J, Wang C, He M, Dou L, Huang X, Li T (2019) Comprehensive characterization of pore and throat system for tight sandstone reservoirs and associated permeability determination method using SEM, rate-controlled mercury and high pressure mercury. J Pet Sci Eng 174:514–524

Heriawan MN, Koike K (2015) Coal quality related to microfractures identified by CT image analysis. Int J Coal Geol 140:97–110

Huang L, Ning Z, Wang Q, Ye H, Chen Z, Sun Z, Sun F, Qin H (2018) Enhanced gas recovery by CO 2 sequestration in marine shale: a molecular view based on realistic kerogen model. Arab J Geosci 11(15):404

Hughes JD (2013) Energy: a reality check on the shale revolution. Nature 494(7437):307–308

Kaufmann J, Loser R, Leemann A (2009) Analysis of cement-bonded materials by multi-cycle mercury intrusion and nitrogen sorption. J Colloid Interface Sci 336(2):730–737

Lai J, Wang G, Wang Z, Chen J, Pang X, Wang S, Zhou Z, He Z, Qin Z, Fan X (2018) A review on pore structure characterization in tight sandstones. Earth Sci Rev 177:436–457 http://www.sciencedirect.com/science/article/pii/S0012825217305226

Li Z, Liu D, Cai Y, Ranjith P, Yao Y (2017) Multi-scale quantitative characterization of 3-D pore-fracture networks in bituminous and anthracite coals using FIB-SEM tomography and X-ray μ-CT. Fuel 209:43–53

Liu X, Wang J, Ge L, Hu F, Li C, Li X, Yu J, Xu H, Lu S, Xue Q (2017) Pore-scale characterization of tight sandstone in Yanchang Formation Ordos Basin China using micro-CT and SEM imaging from nm-to cm-scale. Fuel 209:254–264

Loucks RG, Reed RM, Ruppel SC, Jarvie DM (2009) Morphology, genesis, and distribution of nanometer-scale pores in siliceous

mudstones of the Mississippian Barnett Shale. J Sediment Res 79(12):848–861

Marszałek M, Alexandrowicz Z, Rzepa G (2014) Composition of weathering crusts on sandstones from natural outcrops and architectonic elements in an urban environment. Environ Sci Pollut Res 21(24):14023–14036

Mathews JP, Campbell QP, Xu H, Halleck P (2017) A review of the application of X-ray computed tomography to the study of coal. Fuel 209:10–24 http://www.sciencedirect.com/science/article/pii/S0016236117309419

Munawar MJ, Lin C, Cnudde V, Bultreys T, Dong C, Zhang X, De Boever W, Zahid MA, Wu Y (2018) Petrographic characterization to build an accurate rock model using micro-CT: case study on low-permeable to tight turbidite sandstone from Eocene Shahejie Formation. Micron 109:22–33

Nelson PH (2009) Pore-throat sizes in sandstones, tight sandstones, and shales. AAPG Bull 93(3):329–340

Ougier-Simonin A, Renard F, Boehm C, Vidal-Gilbert S (2016) Microfracturing and microporosity in shales. Earth Sci Rev 162: 198–226 http://www.sciencedirect.com/science/article/pii/S0012825216302914

Schieber J (2010) Common themes in the formation and preservation of intrinsic porosity in shales and mudstones-illustrated with examples across the Phanerozoic. Proc., SPE Unconventional Gas Conference

Song L, Ning Z, Duan L (2018) Research on reservoir characteristics of Chang7 tight oil based on nano-CT. Arab J Geosci 11(16):472

Vázquez MA, Galán E, Ortiz P, Ortiz R (2013) Digital image analysis and EDX SEM as combined techniques to evaluate salt damp on walls. Constr Build Mater 45:95–105

Washburn EW (1921) The dynamics of capillary flow. Phys Rev 17(3): 273–283

Whitney DL, Evans BW (2010) Abbreviations for names of rock-forming minerals. Am Mineral 95(1):185–187

Xi K, Cao Y, Haile BG, Zhu R, Jahren J, Bjørlykke K, Zhang X, Hellevang H (2016) How does the pore-throat size control the reservoir quality and oiliness of tight sandstones? The case of the lower cretaceous Quantou Formation in the southern Songliao Basin, China. Mar Pet Geol 76:1–15

Yang F, Ning Z, Liu H (2014) Fractal characteristics of shales from a shale gas reservoir in the Sichuan Basin, China. Fuel 115:378–384

Yang F, Ning Z, Wang Q, Zhang R, Krooss BM (2016) Pore structure characteristics of lower Silurian shales in the southern Sichuan Basin, China: insights to pore development and gas storage mechanism. Int J Coal Geol 156:12–24

Zhao H, Ning Z, Wang Q, Zhang R, Zhao T, Niu T, Zeng Y (2015) Petrophysical characterization of tight oil reservoirs using pressure-controlled porosimetry combined with rate-controlled porosimetry. Fuel 154:233–242

Zhao H, Ning Z, Zhao T, Zhang R, Wang Q (2016) Effects of mineralogy on petrophysical properties and permeability estimation of the Upper Triassic Yanchang tight oil sandstones in Ordos Basin, Northern China. Fuel 186:328–338 http://www.sciencedirect.com/science/article/pii/S0016236116308365

Zhao T, Li X, Ning Z, Zhao H, Zhang J, Zhao W (2018) Pore structure and adsorption behavior of shale gas reservoir with influence of maturity: a case study of lower Silurian Longmaxi formation in China. Arab J Geosci 11(13):353

Zou C (2017) Unconventional petroleum geology. Elsevier, Amsterdam